Final Project - TALENT 2017 at ECT*

Structure of the Oxygen Isotopes

T. Djärv, N. Gavrielov, L. Riz

(Dated: August 22, 2017)

Our abstract.

INTRODUCTION OF OUR THEORETICAL FRAMEWORK

The oxygen isotopes have been widely investigated [for a review see 1]. To describe their low lying spectrum within the shell model, different model spaces and interactions are used, starting from an ^{16}O core with extra neutrons in the *sd*-shell [2–5], adding the lower *p*-shell for core-excitation (intruder states) with particle-hole configurations [6] and incorporating the *pf*-shell as well [7].

In this work we investigate the structure of the $^{18-28}$O isotopes, both even and odd, by examining their low-lying states. This is done by developing our own shell model program and comparing its results to the NushellX@MSU program [8].

We use an ^{16}O core, having 8 protons and 8 neutron at the *s*-*p*-shells, $(0s_{1/2}, 0p_{3/2}, 0p_{1/2})$. More neutrons are then excited in the *sd*-shell $(0d_{5/2}, 1s_{1/2}, 0d_{3/2})$, which serves as our model space. We use all possible configurations in these orbits and work in a harmonic oscillator basis with spin-orbit splitting. The Hamiltonian reads

$$\hat{H} = \hat{H}_0 + \hat{H}_I, \tag{1}$$

for

$$\hat{H}_0 = \sum_p \epsilon_p \hat{n}_p, \tag{2}$$

the one-body Hamiltonian, where $\hat{n}_p = \hat{a}_p^\dagger \hat{a}_p$ is the number operator for the spherical orbit p with quantum numbers (n_p, ℓ_p, j_p, m_p) and $\epsilon_p = \langle p|h_0|p\rangle$ are the single-particle energies (SPE). The interaction part reads

$$\hat{H}_I = \sum_{p<q=1}^{N} \sum_{r<s=1}^{N} V(p,q;r,s)\hat{T}(p,q;r,s), \tag{3}$$

with

$$\hat{T}(p,q;r,s) = \hat{a}_p^\dagger \hat{a}_q^\dagger \hat{a}_r \hat{a}_s, \tag{4}$$

$\hat{H}_I$ is given in M-scheme and is the two-body density operator for nucleon pairs in orbits p, q and r, s coupled to the total spin projection M, where N is the number of particles in the configuration. In J-scheme $\hat{H}_I$ reads

$$\hat{H}_I = \sum_{a\le b,c\le d} \sum_{JT} V_{J,T}(p,q;r,s)\hat{T}_{J,T}(p,q;r,s), \tag{5}$$

where $\hat{T}_{J,T}(p,q;r,s)$ is the scalar two-body density operator for nucleon pairs in orbits p, q and r, s coupled to spin quantum numbers J, M and isospin quantum numbers T, T_z [5]. Here the appropriate quantum numbers are (n_i, ℓ_i, j_i), $i \in \{a, b, c, d\}$. The transformation between the two-body matrix elements (TBME) from J- to M-scheme reads

$$\begin{aligned} V(p,q;r,s) &= \langle j_p, m_p; j_q, m_q|V|j_r, m_r; j_s, m_s\rangle \\ &= \mathcal{N}_{pq}\mathcal{N}_{rs} \sum_J \langle j_p, m_p; j_q, m_q|JM\rangle \langle j_r, m_r; j_s, m_s|JM\rangle \\ &\quad \times \langle (j_p, j_q)J||V||(j_r, j_s)J\rangle \, \delta_{m_p+m_q, m_r+m_s}, \end{aligned} \tag{6}$$

where other quantum numbers are implicitly implied. Here we have used the Wigner-Eckart theorem with the fact that V is a rank-zero tensor. Furthermore, $\langle j_a, m_a; j_b, m_b|JM\rangle$ is a Clebsch-Gordan coefficient, $\mathcal{N}_{pq}$ ($\mathcal{N}_{rs}$) is a normalization factor and is equal $\sqrt{2}$ if $p = q$ ($r = s$) with only even values of J and 1 if $p \neq q$ ($r \neq s$).

We use the SPE and TBME of the USDB interaction [5] and work in M-scheme. The SPE values and order are given in Table I. The TBME for $A = 18$ are given in [5] in J-scheme for $T = 1, 0$ in Tables I and II, respectively. As was done for the USD interaction [3], the SPE are taken to be mass independent and for the TBME we employ a mass dependence of the form

$$V(p,q;r,s)(A) = \left(\frac{18}{A}\right)^p V(p,q;r,s)(A = 18), \tag{7}$$

with $p = 0.3$. This qualitative mass dependence is expected from the evaluation of a medium-range interaction with harmonic-oscillator radial wave functions. It also defines TBME for other A values in the *sd*-shell.

Using the single-particle states (SPS) we construct the appropriate slater determinants according to the number of particles which we place in the *sd*-shell. This enables us to construct expectation values of the Hamiltonian (1) and diagonalize it to obtain the energies.

In this work we represent a new shell-model code, compare it with NushellX results and conduct further investigation of the oxygen isotopes' wave functions using NushellX.

TABLE I. Single particle energies of the *sd*-shell in the M-scheme basis with their corresponding quantum numbers: N, the principle quantum number; ℓ, the orbital angular momentum; J, the total angular momentum; M_j, the total angular momentum projection on the z axis.

index	N	ℓ	J	M_j	SPE
1	1	0	1	$-1/2$	-3.20790
2	1	0	1	$+1/2$	-3.20790
3	0	2	3	$-3/2$	2.11170
4	0	2	3	$-1/2$	2.11170
5	0	2	3	$+1/2$	2.11170
6	0	2	3	$+3/2$	2.11170
7	0	2	5	$-5/2$	-3.92570
8	0	2	5	$-3/2$	-3.92570
9	0	2	5	$-1/2$	-3.92570
10	0	2	5	$+1/2$	-3.92570
11	0	2	5	$+3/2$	-3.92570
12	0	2	5	$+5/2$	-3.92570

LNLTSHELL

Throughout this project a simple shell-model code, called "LNLTShell", has been developed in python. The main goal of this shell-model is to be able reproduce the oxygen isotopes spectra in the sd-shell.

A nuclear shell-model code approximate a spectrum for an atomic Nucleus of with A nucleons by assuming a frozen core of A_{core} nucleons, and then solves the many-body Schrödinger equation for a group of $n = A - A_{\text{core}}$ valence nucleons.

The program starts by parsing the argument list. There are six different arguments:

-n n: Used to specify number of valence nucleons.

-M M: Used for total-M restriction, discussed below.

-of filename: To specify what json file contains the shells.

-os bool: To turn the pairing basis on and off.

-if filename: To specify what file contains the two-body matrix elements.

-o filename: To specify what file to write the output to.

observe that -of and -if are mutually exclusive.

The first thing the code does after parsing the arguments is setting up the single particle basis. This is done either by reading them directly from the m-scheme matrix element file or by constructing them from given shells it reads in a given json file.

When the single particle basis is determined, all possible Slater determinants for the valence nucleons are constructed to form the many-body basis. This is done by constructing all unique combinations of n single particle states, each such combination representing a Slater determinant. After the many-body basis is constructed, it is possible to apply total M-restriction to exploit that the used Hamiltonian is a spherical scalar and therefore block-diagonal in total M. This is done by removing all Slater determinants that do not have the desired total M.

The many-body Hamiltonian matrix is constructed in the class TwoBodyOperator, by acting with $\langle a,b|\,V\,|c,d\rangle_{AS}\, a_a^\dagger a_b^\dagger a_d a_c$ repeatedly for different values of a, b, c, d on all the Slater determinants in the many-body basis to determine which states differ with up to two single-particles states. This process results in a full matrix which then is diagonalized by applying a full diagonalization routine from numpy. This results in list of eigen energies E with associated eigen states $|E,i\rangle$ where i takes care of potential degeneracy.

When the eigenstates to the Hamiltonian has been computed, the total angular momentum of each state is computed by solving $\hbar^2 J(J+1) = \langle E,i|\,\hat{J}^2\,|E,i\rangle$ for each state. The operator $\hat{J}^2$ can be divided in a two-body and a one-body operator, from which a many-body matrix can be obtained with the same machinery as the full Hamiltonian matrix can be obtained.

For each state shell-occupation number is determined by the application of

$$\langle E,i|\,n_k\,|E,i\rangle = \langle E,i|\sum_{m=-j}^{j} a_{k,m}^\dagger a_{k,m}\,|E,i\rangle \qquad (8)$$

where k represents the shell, and j is associated by k.

The program writes the results to the screen and optionally to a user specified file, where the single-particle basis, the many-body basis and the eigen-spectrum of the Hamiltonian.

Different interactions can be provided in two different ways. Either by a file which format will be described below, or as a class containing a method get_matrix_element that takes four single particle states as its arguments. The matrix element file starts by stating how many single-particle states there are, and then continues listing them together with the single-particle energies. There after the file contains a number l representing how many two-body matrix elements there exists, followed by l lines of four integers representing the two-body states on the bra and ket side of the two-body matrix element and one fixed point value with 5 decimals and one hole number.

COMPARISION BETWEEN LNLT_SHELL AND NUSHELLX

To verify that the code descirbed in section works, several isotopes of oxygen were computed with LNLT_shell and compared to the result from NuShellX with the USDB interaction. In table IV,V and VI the eigenenergies of ^{18,19,20}O is compared to the values computed with NuShellX. The energies are relative the ground energy of

^{16}O. There are almost no difference to the given numerical precission, only a few of the higher eigen-values differ slightly. In addition the code seems to correctly assign total angular momentum; the J_L columns are identical with the J_N columns. To illustrate the similarity further, the lowest energies are ploted in figure 1,2 and 3, where also a comparision to experiment is made.

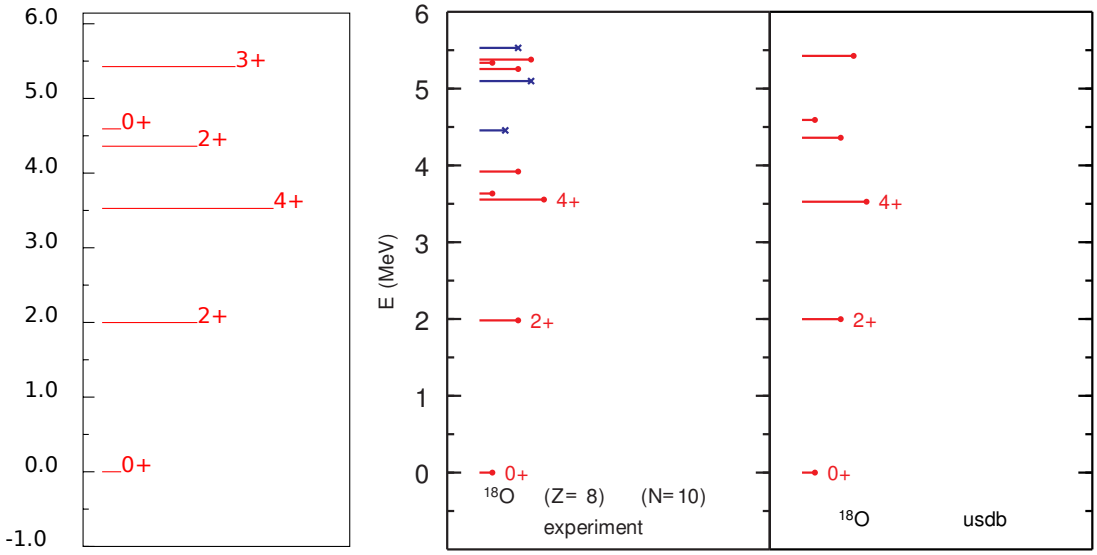

FIG. 1. The lowest energy states of ^{18}O, computed by LNLT_shell to the left compared to the eigenspectrum from experiment and NuShellX to the right

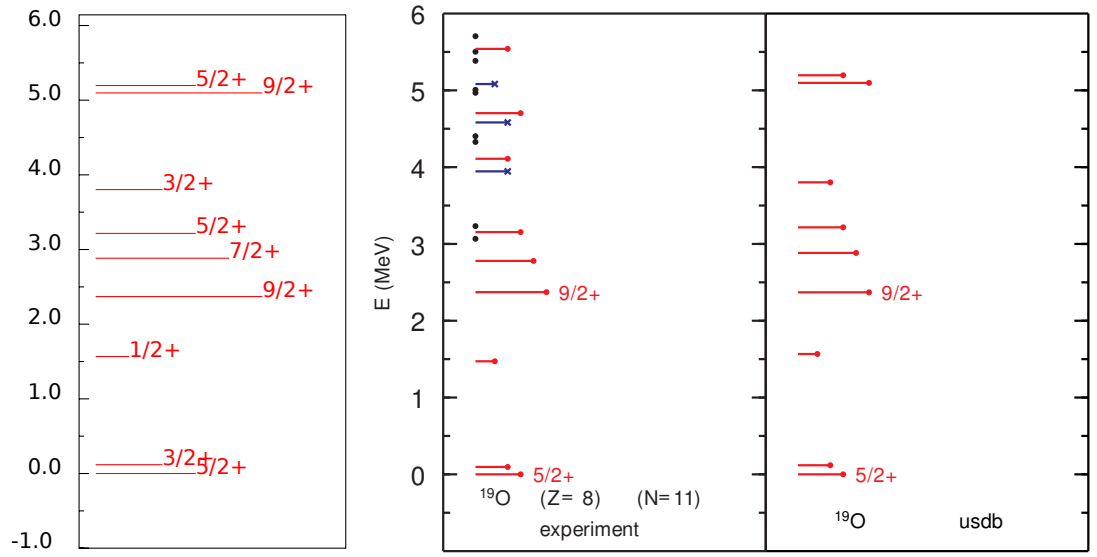

FIG. 2. The lowest energy states of ^{19}O, computed by LNLT_shell to the left compared to the eigenspectrum from experiment and NuShellX to the right

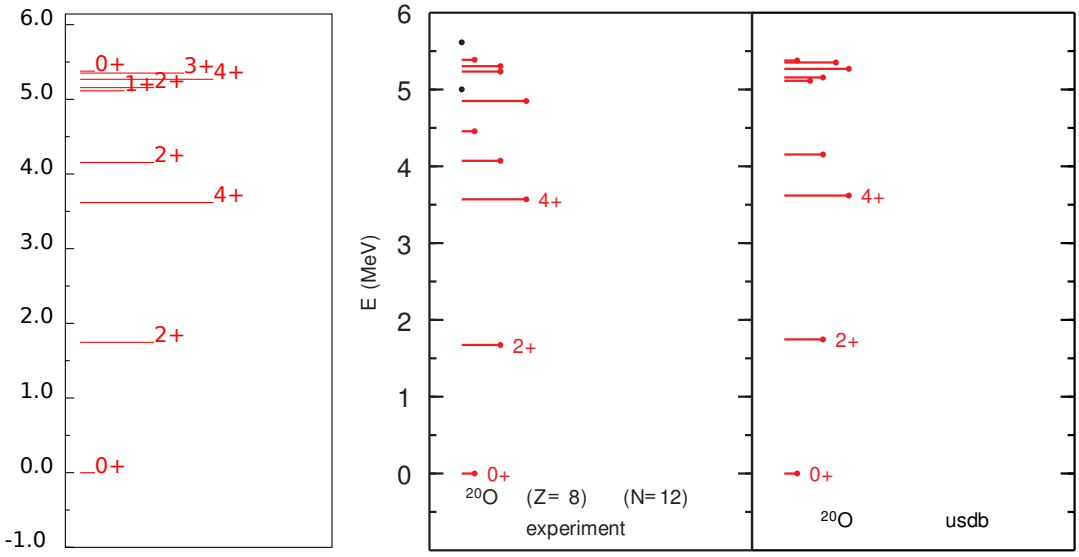

FIG. 3. The lowest energy states of ^{20}O, computed by LNLT_shell to the left compared to the eigenspectrum from experiment and NuShellX to the right

In addition to the eigen-spectrum for each shell-occupation numbers where also computed. In Table VII all the shell-occupation numbers for all 14 states can be viewed, computed both with LNLT_shell and with NuShellX. There are some slight difference, however this can be easily explained with that LNLT_shell outputs higher precision than NuShellX does and thus the difference is moste likely due to rounding errors. In Figs. 4 and 5 the shell occupation for the ground state and the first excited states are visualized, computed by LNLT_shell and NuShellX respectively. Also here there are a slight difference, which still can be explained with rounding errors.

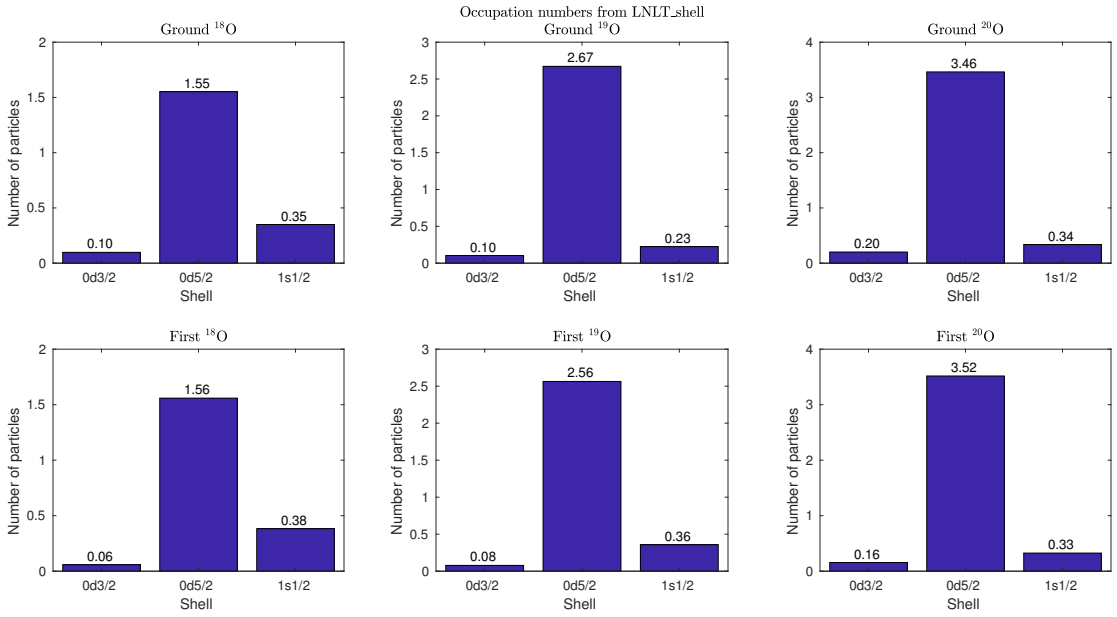

FIG. 4. The occupation numbers of the ground state and first excited state of ^{18,19,20}O as computed by LNLT_shell.

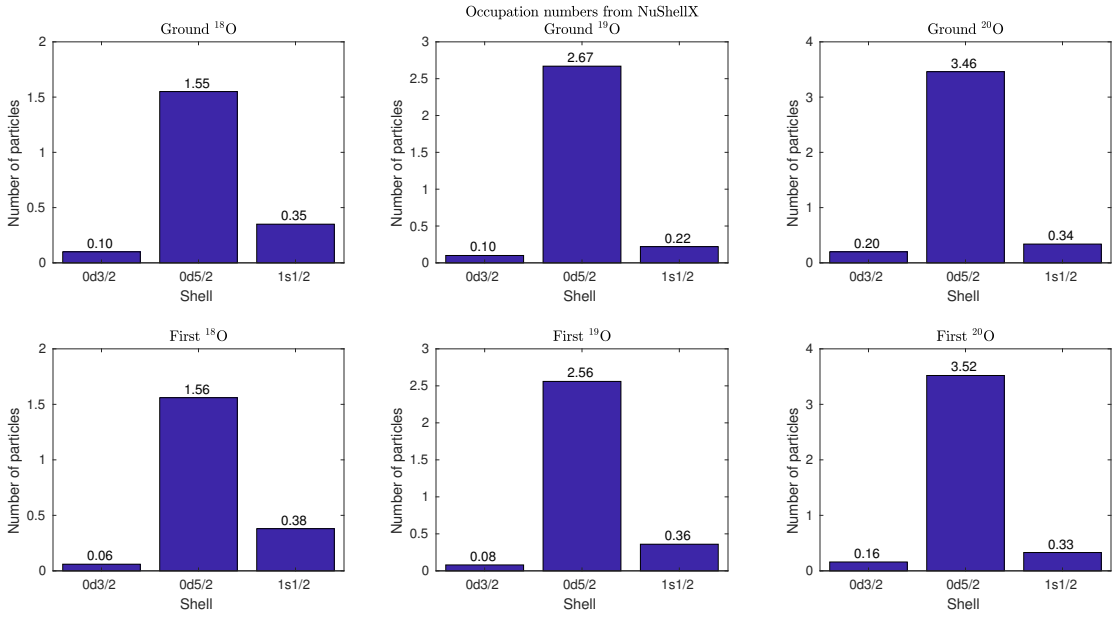

FIG. 5. The occupation numbers of the ground state and first excited state of ^{18,19,20}O as computed by NuShellX.

NUSHELLX

The structure of the wave functions of different levels in the oxygen isotopes is interesting to examine since it can reveal the role of different configurations and orbits. Furthermore, within a given configuration examining different interactions using different observables can be also insightful. In the first subsection we examine using NushellX@MSU the spectra of oxygen isotopes and the capability of different interactions, the USDA, USDB and coupled cluster effective interaction (CCEI) [9] to reproduce spectra. The second subsection is devoted to the study of Fermi and Gamow-Teller β-decay of ^{22}O and how the USDB and CCEI interactions fulfill sum rules. The third subsection addresses electromagnetic transitions rates for different isotopes and interactions.

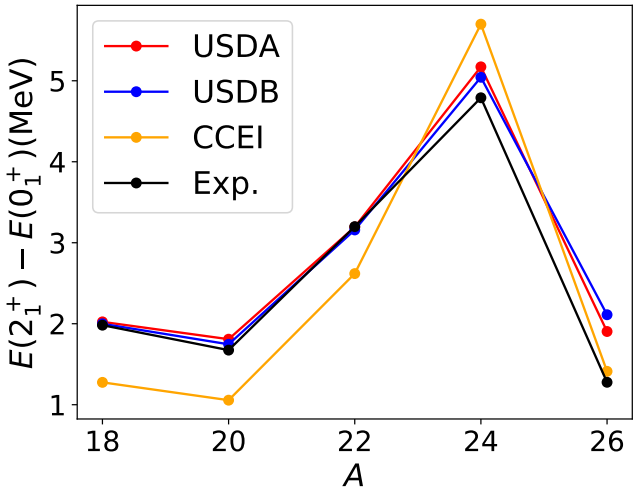

FIG. 6. Excitation energy of the first 2^+ state in oxygen isotopes (even-even).

Oxygen isotopes spectra with different interactions

We analyze how the different interactions reproduce the excitation energy of the first 2^+ state in even-even oxygen isotopes from ^{18}O to ^{26}O and compare to experiment. This is seen in Fig. 6 and gives an indication on the location of the shell closure. The latter arises when the excitation energy from the g.s. to the first excited 2^+ state is at maximum.

The USDA and USDB interactions give similar results, are in good agreement with experimental results and give a good description of the shell closure at ^{24}O. Since USDB has more linear combination of parameters than USDA it generates a better agreement with the experimental results. The CCEI interaction underestimates the excitation energies up to ^{26} oxygen, while at shell closure it emphasize this effect by overestimating the first 2^+ state energy. It is interesting to note that CCEI interactions seems to give a good description in rich neutron isotopes, close to the neutron drip line.

We next explore the spectra of even-odd oxygen isotopes. Among them we analyze the spectrum of ^{19}O since it has the largest amount of experimental data. The results are shown in Fig. 7. Note that the experimen-

tal results show also negative parity states (blue lines), which are not included in our theoretical calculations since we are working in the *sd* model space. For completeness black dots in the experimental panel indicates states which have not been assigned to a definite parity.

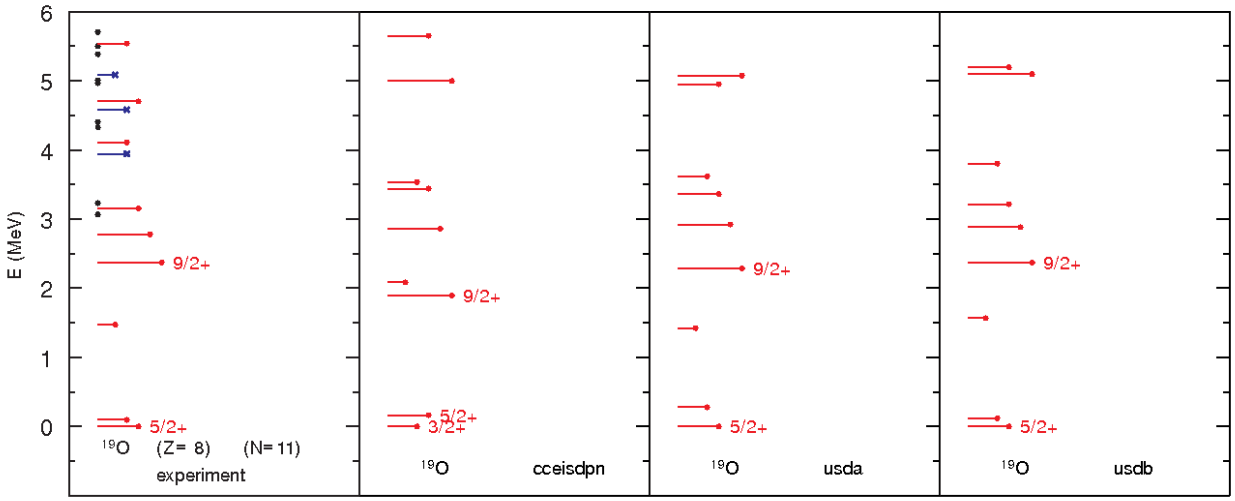

FIG. 7. ^{19}O spectrum with different interactions compared to experiments.

The USDA and USDB reproduce the correct spin orderings, where the USDA yields better results up to the first $1/2^+$ at energy 1.422 MeV and the USDB yields better results from the first $9/2^+$ at energy 2.370 MeV up to the second $3/2^+$ at energy 3.802 MeV. The differences are not significant though and further tests for comparison could be electromagnetic transition rates. The CCEI exchanges the order of the first $3/2^+$ with the g.s. and the order of the first $9/2^+$ and the first $1/2^+$, causing both pairs to be nearly degenerate. The former case is reasonable since the g.s. and the first $3/2^+$ are nearly degenerate, however the latter case exhibits a larger discrepancy from experiment.

Fermi and Gamow-Teller β-decay of ^{22}O

On top of energies, it is insightful to examine other observables in order to understand better the differences between different interactions. We analyze the β-decay of ^{22}O to ^{22}F. We perform the calculations using NushellX for the USDB and CCEI interactions.

Both interactions fulfill the theoretical Fermi sum rule, but in different ways. The contribution of the CCEI interaction to the Fermi sum rule b(f) splits among different states: this is because the e interaction has several nearly degenerate levels which mix. The USDB interaction gives all the contribution to b(f) in one single state, which is the isobar analogue of the ^{22}O (is this true? - Ch. 44 Brown's notes). (Anyone has more to say about Gamow-Teller sum rule?)

TABLE II. Sum Rules

	sum rule	CCEI	USDB
sum b(f)	$N_i - Z_i = 6$	5.9993	6.0000
sum qf·b(gt)	$\geq 3 \cdot (N_i - Z_i) = 18$	6.0346	10.0335

Let us compare the results obtained with the two different interactions to the experimental results for the q-value and the half-life. Note that one has to include more than only the default ten levels for each spin state in NushellX in order to get significant results, otherwise too much information is neglected.

TABLE III. q-value and $t_{1/2}$

	exp	CCEI	USDB
q-value [MeV]	6.489	6.847	8.437
$t_{1/2}$ [sec]	2.25	0.478	2.620

The CCEI interaction gives a good description of the q-value, but underestimates the half-life, while the USDB interaction is in good agreement with the experimental value for the half-life, but slightly overestimates the q-value.

$E2$ transitions of the oxygen isotopes

Here we will only investigate the $E2$ between the first 2^+ and the first 0^+, i.e. $B(E2; 2_1^+ \rightarrow 0_1^+)$, using the USDA, USDB and CCEI interactions, given in Fig. 8. For the experimental data there are only three values, however it is notable that they become closer to the theoretical values as neutrons are added, with the largest discrepancy occurring for the ^{18}O isotope. The reason might be due to the fact we are neglecting p-shell core-excitations when using only the sd-shel model space. It was found in [6] that the 0_2^+ should have a dominant $4p-2h$ component. However there are indications that mixing should arise, and perhaps with the 0_1^+. As for the 2_1^+, there might be less mixing with an intruder configuration since the 2_3^+, which has a large intruder component, is high in energy (5.255 MeV) and thus mixes less with the 2_1^+. The problem for mixing of these states due to the truncation in the np–mh sequence is discussed in [10]. Therefore, when close to the ^{16}O core, e.g. at ^{18}O, a some part of the p-shell is missing in the wave function of 0_1^+ rendering less components in the wave functions to connect between the 0_1^+ and the 2_1^+ and hence yielding a smaller $B(E2)$ value. As neutrons are added to the ^{16}O core, the p-shell core-excitations move to higher energy and mix less with the low-lying states, then the sd-shell model space becomes a better approximation. As seen in Fig. 8, this is correct for all three interactions which operate in the sd-shell. Although the CCEI does not reproduce energies as well as USDA and USDB, it gives a slightly better approximation for the $B(E2; 2_1^+ \rightarrow 0_1^+)$. Yet, the differences are minor and other observables should be examined.

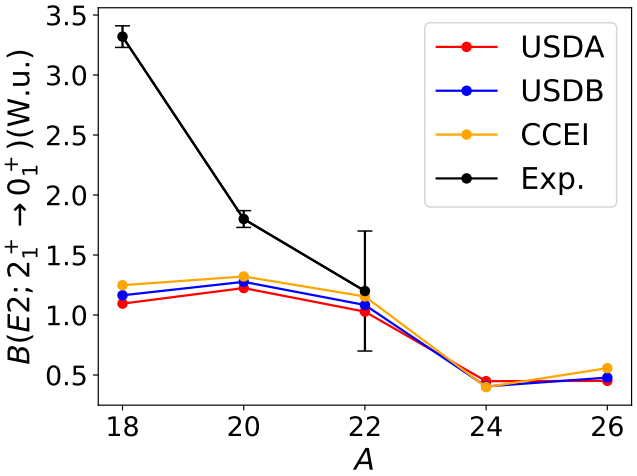

FIG. 8. $B(E2; 2^+ \rightarrow 0^+)$ of experimental (black), the USDA (red), USDB (blue) and CCEI (orange) interactions for $^{18-26}$O.

CONCLUSIONS AND OUTLOOK

Tables

TABLE IV. The energy spectrum of ^{18}O computed with LNLT_shell (to the left) compared to NuShellX result (to the right). J_L is computed with LNLT_shell while J_N are computed with NuShellX.

Nr	E	J_L	E_{NuShellX}	J_N
1	-11.932	0	-11.932	0
2	-9.933	2	-9.933	2
3	-8.405	4	-8.405	4
4	-7.572	2	-7.572	2
5	-7.339	0	-7.339	0
6	-6.505	3	-6.505	3
7	-2.912	4	-2.912	4
8	-2.051	2	-2.050	2
9	-1.162	1	-1.162	1
10	-0.991	3	-0.991	3
11	-0.901	2	-0.901	2
12	-0.577	1	-0.577	1
13	3.077	0	3.077	0
14	4.288	2	4.288	2

TABLE V. The energy spectrum of ^{19}O computed with LNLT_shell (to the left) compared to NuShellX result (to the right). J_L is computed with LNLT_shell while J_N are computed with NuShellX.

Nr	E	J_L	E_{NuShellX}	J_N	Nr	E	J_L	E_{NuShellX}	J_N
1	-15.956	5/2	-15.956	5/2	20	-5.247	9/2	-5.247	9/2
2	-15.838	3/2	-15.838	3/2	21	-5.211	7/2	-5.211	7/2
3	-14.389	1/2	-14.389	1/2	22	-5.155	5/2	-5.155	5/2
4	-13.586	9/2	-13.586	9/2	23	-4.713	1/2	-4.713	1/2
5	-13.072	7/2	-13.072	7/2	24	-4.676	3/2	-4.676	3/2
6	-12.74	5/2	-12.740	5/2	25	-4.001	5/2	-4.002	5/2
7	-12.153	3/2	-12.153	3/2	26	-3.379	3/2	-3.379	3/2
8	-10.859	9/2	-10.859	9/2	27	-3.348	7/2	-3.348	7/2
9	-10.759	5/2	-10.759	5/2	28	-1.363	5/2	-1.363	5/2
10	-9.875	3/2	-9.875	3/2	29	-0.854	9/2	-0.854	9/2
11	-8.758	7/2	-8.758	7/2	30	-0.392	7/2	-0.392	7/2
12	-8.095	1/2	-8.095	1/2	31	0.105	1/2	0.105	1/2
13	-8.088	5/2	-8.095	1/2	32	0.755	1/2	0.755	1/2
14	-7.97	11/2	-7.970	11/2	33	1.401	3/2	1.401	3/2
15	-7.118	3/2	-7.118	3/2	34	1.41	5/2	1.401	3/2
16	-6.5	7/2	-6.500	7/2	35	1.689	5/2	1.689	5/2
17	-6.361	5/2	-6.361	5/2	36	2.037	3/2	2.037	3/2
18	-6.184	9/2	-6.184	9/2	37	5.946	3/2	5.946	3/2
19	-5.597	3/2	-5.597	3/2	-	-	-	-	-

TABLE VI. The energy spectrum of ^{20}O computed with LNLT_shell (to the left) compared to NuShellX result (to the right). J_L is computed with LNLT_shell while J_N are computed with NuShellX.

Nr	E	J_L	E_{NuShellX}	J_N	Nr	E	J_L	E_{NuShellX}	J_N	Nr	E	J_L	E_{NuShellX}	J_N
1	-23.632	0	-23.632	0	29	-11.122	2	-11.122	2	57	-5.007	2	-5.007	2
2	-21.886	2	-21.886	2	30	-11.07	0	-11.070	0	58	-4.906	0	-4.906	0
3	-20.013	4	-20.013	4	31	-10.93	4	-10.930	4	59	-4.684	4	-4.684	4
4	-19.478	2	-19.478	2	32	-10.714	4	-10.714	4	60	-4.18	3	-4.180	3
5	-18.518	1	-18.518	1	33	-10.544	3	-10.544	3	61	-4.043	0	-4.043	0
6	-18.475	2	-18.475	2	34	-10.451	1	-10.450	1	62	-3.508	2	-3.508	2
7	-18.363	4	-18.363	4	35	-10.305	6	-10.305	6	63	-3.492	4	-3.492	4
8	-18.28	3	-18.280	3	36	-10.205	2	-10.205	2	64	-3.23	3	-3.230	3
9	-18.254	0	-18.254	0	37	-9.862	2	-9.862	2	65	-2.984	3	-2.984	3
10	-16.248	4	-16.248	4	38	-9.595	4	-9.595	4	66	-2.953	1	-2.953	1
11	-16.163	5	-16.163	5	39	-9.533	3	-9.533	3	67	-2.904	5	-2.904	5
12	-15.455	2	-15.455	2	40	-9.359	0	-9.359	0	68	-2.885	2	-2.885	2
13	-15.052	4	-15.052	4	41	-9.141	1	-9.141	1	69	-2.319	4	-2.319	4
14	-14.996	2	-14.996	2	42	-8.623	3	-8.623	3	70	-2.228	2	-2.228	2
15	-14.865	3	-14.865	3	43	-8.549	2	-8.549	2	71	-2.103	0	-2.103	0
16	-13.963	0	-13.963	0	44	-8.491	5	-8.491	5	72	-1.114	1	-1.114	1
17	-13.524	1	-13.524	1	45	-8.186	2	-8.186	2	73	-0.36	2	-0.360	2
18	-13.52	2	-13.524	1	46	-7.814	3	-7.814	3	74	-0.332	3	-0.332	3
19	-13.241	6	-13.241	6	47	-7.713	4	-7.713	4	75	0.913	4	0.913	4
20	-13.229	3	-13.229	3	48	-7.517	1	-7.517	1	76	1.366	3	1.365	3
21	-12.508	2	-12.508	2	49	-7.15	4	-7.150	4	77	1.826	2	1.826	2
22	-12.314	5	-12.314	5	50	-6.934	2	-6.934	2	78	3.481	2	3.481	2
23	-12.231	1	-12.231	1	51	-6.459	6	-6.459	6	79	4.029	1	4.030	1
24	-11.991	5	-11.991	5	52	-6.305	2	-6.306	2	80	4.163	1	4.163	1
25	-11.849	1	-11.849	1	53	-6.264	4	-6.264	4	81	7.643	0	7.643	0
26	-11.637	4	-11.637	4	54	-5.826	3	-5.826	3	-	-	-	-	-
27	-11.426	3	-11.426	3	55	-5.351	1	-5.351	1	-	-	-	-	-
28	-11.267	3	-11.267	3	56	-5.133	5	-5.133	5	-	-	-	-	-

TABLE VII. The occupation numbers for ^{18}O, computed with LNLT_shell to the left and NuShellX to the right

State	$0d_{3/2}$	$0d_{5/2}$	$1s_{1/2}$	Total	NuShellX	$0d_{3/2}$	$0d_{5/2}$	$1s_{1/2}$	Total
1	0.098	1.552	0.35	2.0	1	0.1	1.55	0.35	2.0
2	0.058	1.559	0.383	2.0	2	0.06	1.56	0.38	2.0
3	0.063	1.937	0.0	2.0	3	0.06	1.94	0.0	2.0
4	0.017	1.363	0.621	2.0	4	0.02	1.36	0.62	2.0
5	0.003	0.353	1.644	2.0	5	0.0	0.35	1.64	1.99
6	0.01	1.0	0.99	2.0	6	0.01	1.0	0.99	2.0
7	0.937	1.063	0.0	2.0	7	0.94	1.06	0.0	2.0
8	0.99	0.942	0.068	2.0	8	0.99	0.94	0.07	2.0
9	1.0	0.994	0.006	2.0	9	1.0	0.99	0.01	2.0
10	0.99	1.0	0.01	2.0	10	0.99	1.0	0.01	2.0
11	0.958	0.116	0.926	2.0	11	0.96	0.12	0.93	2.01
12	1.0	0.006	0.994	2.0	12	1.0	0.01	0.99	2.0
13	1.899	0.095	0.007	2.0	13	1.9	0.09	0.01	2.0
14	1.977	0.021	0.002	2.0	14	1.98	0.02	0.0	2.0

[1] B. A. Brown, Int. J. Mod. Phys. E **26**, 1740003 (2017).
[2] T. T. S. Kuo and G. E. Brown, Nucl. Phys. **85**, 40 (1966).
[3] B. H. Wildenthal, Prog. Part. Nucl. Phys. **11**, 5 (1984).
[4] B. A. Brown and B. H. Wildenthal, Annu. Rev. Nucl. Part. Sci. **38**, 29 (1988).
[5] B. A. Brown and W. A. Richter, Phys. Rev. C **74**, 034315 (2006).
[6] R. L. Lawson, F. J. D. Serduke, and H. T. Fortune, Phys. Rev. C **14**, 1245 (1976).
[7] Y. Utsuno, T. Otsuka, T. Mizusaki, and M. Honma, Phys. Rev. C **60**, 054315 (1999).
[8] B. A. Brown and W. Rae, Nucl. Data Sheets **120**, 115 (2014).

[9] G. R. Jansen, M. D. Schuster, A. Signoracci, G. Hagen, and P. Navrátil, Phys. Rev. C **94**, 011301 (2016).
[10] E. K. Warburton, B. A. Brown, and D. Millener, Phys. Lett. B **293**, 7 (1992).